American Mineralogist, Volume 63, pages 1074–1087, 1978

Amphiboles in andesite and basalt: II. Stability as a function of P–T–fH_2O–fO_2[1]

J. C. ALLEN

Department of Geology and Geography, Bucknell University
Lewisburg, Pennsylvania 17837

AND A. L. BOETTCHER

Institute of Geophysics and Planetary Physics
and The Department of Earth and Space Sciences
University of California at Los Angeles
Los Angeles, California 90024

Abstract

The stabilities of amphiboles at high pressures in an andesite and a basalt have been determined in the presence of H_2O–CO_2 vapors for values of mole fraction of H_2O in the vapor (X^VH_2O) of 1.0, 0.75, 0.5, and 0.25. The maximum thermal stability of amphibole in the andesite is about 970°C in the range of 10 to 20 kbar and X^VH_2O of ~0.75. Comparable data for the basalt are 1050°C from 10 to 15 kbar and X^VH_2O of 0.25. The maximum pressure stability of amphibole is 21.5 kbar at X^VH_2O ~1.0 in the andesite and 20.5 kbar at X^VH_2O ~1.0 in the basalt. Electron microprobe analyses are presented for orthopyroxenes, clinopyroxenes, amphiboles, garnets, and glasses synthesized over a range of pressures, temperatures, X^VH_2O, and bulk composition. Most of the amphiboles are nepheline-normative, calciferous, and tschermakitic.

These data on the chemistry of amphiboles and the temperature-pressure conditions over which they are stable are consistent with our hypothesis in which andesites of the circum-Pacific zone are derived by amphibole-liquid equilibria from basaltic magma.

Introduction

Water plays a prominent role in the genesis and evolution of andesites and kindred rocks in orogenic zones at the sites of plate collisions involving oceanic crust. Water in subducting oceanic crust is, to a major degree, contained in amphiboles until the subducting plate attains a depth at which these phases melt or transform to denser (*e.g.*, garnet-bearing) assemblages. In addition, the fractionation of amphiboles in hydrous magmas is, at least conceptually, a mechanism by which andesites can evolve from basaltic magmas. Thus, it is of paramount importance to understand the conditions under which amphiboles exist.

As a first step in solving this problem, we (Allen *et al.*, 1975) experimentally established the stabilities of amphiboles in an andesite, three basalts, and an olivine nephelinite in the presence of nearly pure H_2O vapor at values of oxygen fugacity (fO_2) approximately those of Fe_3O_4–Fe_2O_3, Ni–NiO, and Fe_3O_4–FeO from 10 to 36 kbar. Although these experiments are valuable in that they place certain limits on the stability of amphiboles, these conditions of very high H_2O fugacity (fH_2O) are not commonly attained in deep-seated magmas. This study extends our investigation of the stability of amphiboles in andesitic and basaltic magmas at high pressures to lower and more realistic values of fH_2O by using H_2O–CO_2 vapors. CO_2 is, of course, a major component in many rocks (*e.g.*, kimberlites), but the main use of CO_2 in these experiments is as a diluent, lowering the fH_2O. This method of lowering fH_2O would mimic conditions in nature where a vapor may not be present, except that the vapor in our experiments does incongruently dissolve small proportions of the crystalline phases.

[1] Institute of Geophysics and Planetary Physics Contribution No. 1765.

0003-004X/78/1112-1074$02.00

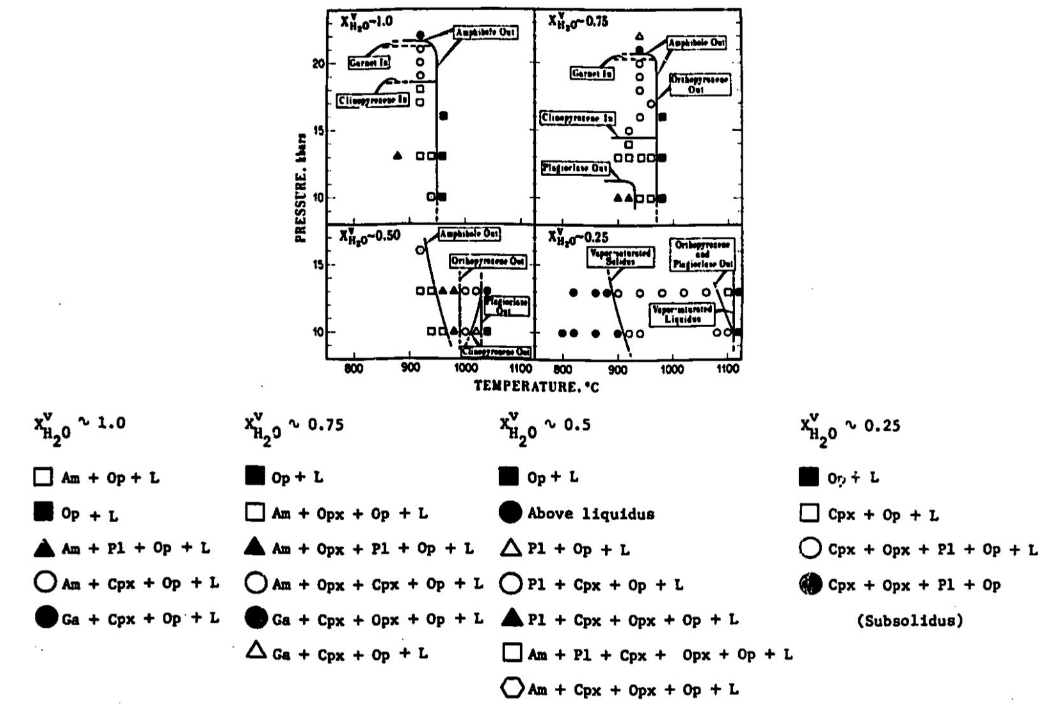

Fig. 1. Crystallization sequence for Mt. Hood andesite at X^VH_2O ~ 1.0, 0.75, 0.5, and 0.25. All assemblages coexist with vapor. Abbreviations: Am–amphibole; Cpx–clinopyroxene; Ga–garnet; L–glass interpreted to be quenched liquid; M–micaceous mineral; Ol–olivine; Op–opaque mineral; Opx–orthopyroxene; Pl–plagioclase; q–interpreted to have crystallized during the quench; ?–questionable; ( )–trace amount.

Experimental methods

Starting materials

Starting mixes were prepared from a Mt. Hood andesite and a 1921 Kilauea olivine tholeiite, two of the five materials used in our earlier experiments (see Allen *et al.*, 1975 for chemical compositions and norms). The melting relationships of these rocks at other conditions have been investigated by other workers (for references, see Allen *et al.*, 1975, p. 1070; Helz, 1976).

Capsules and buffer

All samples were crushed to −200 mesh under acetone, dried in an oven at 110°C, and stored in sealed vials over KOH in a dessicator. The samples were then encapsulated with 20 percent (weight) H_2O into welded Ag–Pd capsules of 1.5 mm I.D. for the experiments with X^VH_2O ~ 1.0. For experiments with H_2O-CO_2 vapors, mixtures of H_2O and $Ag_2C_2O_4$ appropriate to yield the desired values of X^VH_2O were sealed into welded Pt capsules of 1.5 mm I.D. Because our experiments were at near-liquidus temperatures, these X^VH_2O values are only approximate, resulting from the differential solubility of H_2O and CO_2 in silicate melts. Hydrogen fugacity was buffered at Fe_3O_4–Fe_2O_3–H_2O (M–H) conditions to prevent the precipitation of carbon from the vapor that would result in an unknown but higher H_2O/CO_2. These techniques are described in detail by Boettcher *et al.* (1973). Optical and X-ray diffraction techniques were used to ensure that the M–H assemblage lasted the duration of the experiments. Leaks in the inner capsules during the experiment were determined afterward by comparing pre- and post-experiment capsule weights and by puncturing and then reweighing the capsule. Unpublished experimental evidence from our laboratory reveals that loss of iron to the Pt capsule is negligible under these conditions of high fO_2, whereas at lower fO_2, under M–W and N–NO buffer conditions, loss of iron is a serious problem (Stern and Wyllie, 1975).

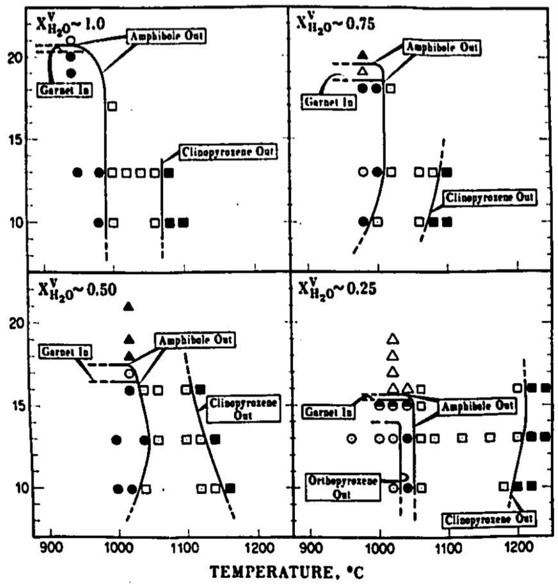

$X^V_{H_2O}$ ∿ 1.0
- ■ Op + L
- □ Cpx + Op + L
- ● Am + Cpx + Op + L
- ○ Ga + Cpx + Op + L

$X^V_{H_2O}$ ∿ 0.75
- ■ Op + L
- □ Cpx + Op + L
- ● Am + Cpx + Op + L
- ○ Am + Cpx + Pl + Op + L
- ▲ Ga + Cpx + Op + L
- △ Am + Cpx + Ga + Op + L

$X^V_{H_2O}$ ∿ 0.5
- ■ Op + L
- □ Cpx + Op + L
- ● Am + Cpx + Op + L
- ○ Am + Ga + Cpx + Op + L
- ▲ Ga + Cpx + Op + L

$X^V_{H_2O}$ ∿ 0.25
- ■ Op + L
- □ Cpx + Op + L
- ● Am + Cpx + Op + L
- ○ Am + Cpx + Pl + Opx + Op + L
- ◒ Am + Cpx + Pl + Op + L
- ▲ Ga + Cpx + Op + L

Fig. 2. Crystallization sequence for 1921 Kilauea olivine tholeiite at X^VH_2O ~ 1.0, 0.75, 0.5, and 0.25. All assemblages coexist with vapor. Trace amounts of olivine occur in some runs (see Table 1). See Fig. 1 for abbreviations.

Apparatus

All experiments used a piston-cylinder apparatus and furnace assembly similar to that described in Allen *et al.* (1975), except that a Pyrex glass sleeve was inserted between the talc and graphite cylinders, and a single boron nitride cylinder replaced the boron nitride and talc cylinders used in our earlier work.

Run procedure

A pressure of at least one kbar below that to be maintained during the run was first applied to the furnace assembly. Then the temperature was increased to the appropriate value over a period of about seven minutes, and the pressure was increased to the desired value. Synthesis runs lasted between three and 24 hours. To reverse the amphibole-out curves, two-stage runs were made in which temperatures were initially held above and then lowered into the stability field of amphibole, as tabulated in Table 1.[2] A similar procedure served to reverse the vapor-saturated liquidi.

Identification and description of phases

See Part I (Allen *et al.*, 1975, p. 1072).

[2] To obtain a copy of Table 1, order Document AM-78-089 from the Business Office, Mineralogical Society of America, 1909 K Street, NW, LL 1000, Washington, DC 20006. Please remit $1.00 in advance for the microfiche. Or write Dr. A. L. Boettcher, Institute of Geophysics and Planetary Physics, UCLA, Los Angeles, CA 90024.

Results

Phase relationships

The results of experiments on the two starting materials are presented in Table 1, and the phase relationships are shown in *P–T* projection in Figures 1 and 2. Amphibole is stable in the 1921 Kilauea olivine tholeiite (Fig. 2) under values of X^VH_2O from 1.0 to at least as low as 0.25, and in the Mt. Hood andesite (Fig. 1) at X^VH_2O values of approximately 1.0, 0.75, and 0.50, but not of 0.25, at least not above the vapor-saturated solidus. The amphibole-out curves consist of a high-temperature segment with a rather steep slope and a high-pressure one with a relatively small slope (dP/dT). Amphiboles melt in each of the starting materials at temperatures of the steep segments, and amphibole-bearing assemblages convert to garnet-bearing assemblages at pressures greater than those of the high-pressure segments. Each of the segments of the amphibole-out curves with a relatively small slope probably continues to lower temperatures in the manner shown in Figure 2 ($X^VH_2O \sim 0.25$).

The maximum thermal stability of amphibole in the andesite is 970°C, which is attained at X^VH_2O of ~0.75 (and at 0.50 at 10 kbar). Note that amphibole in this andesitic melt persists to somewhat higher temperatures under these conditions than under any of the conditions reported on in our earlier study using nearly pure H_2O vapors over a wide range of fO_2 (Allen *et al.*, 1975). Maximum pressure stability is 21.5 kbar at $X^VH_2O \sim 1.0$. At a X^VH_2O of ~0.75, orthopyroxene is most abundant at lower pressures and is present only in minor or trace amounts at higher pressures. Clinopyroxene, stable at pressures of 15 kbar and above at X^VH_2O of ~0.75, increases in abundance as orthopyroxene decreases.

The maximum thermal stability of amphibole in

Table 2. Garnet compositions

Analysis Rock	1 Andesite	2 Andesite	3 Andesite	4 Basalt	5 Basalt	6 Basalt	7 Basalt	8 Basalt	9 Basalt
$X^V_{H_2O}$	∿ 1.0	∿ 1.0	∿ 0.75	∿ 0.75	∿ 0.75	∿ 0.50	∿ 0.50	∿ 0.50	∿ 0.50
P, Kbar	22	22	22	20	20	21	21	21	21
T, °C	920	920	940	980	980	1020	1020	1020	1020
SiO_2	41.23	40.62	39.82	41.92	42.72	40.00	41.04	39.55	39.82
TiO_2	0.43	0.51	0.71	0.80	0.91	0.94	0.94	0.85	1.21
Al_2O_3	20.58	20.79	20.82	20.50	19.65	21.49	19.59	20.83	20.54
FeO*	15.11	14.17	16.45	12.40	12.60	14.88	14.08	14.07	13.80
MgO	12.45	13.35	11.06	15.08	14.22	13.41	13.46	13.49	14.22
MnO	0.94	1.47	0.66	0.63	0.72	0.57	0.48	0.52	0.54
CaO	10.78	10.01	9.90	7.24	7.98	7.72	9.71	8.77	7.83
Na_2O	0.01	-	-	0.12	0.12	0.04	0.26	0.05	0.17
K_2O	0.05	0.03	0.05	0.04	0.02	0.01	0.01	0.02	0.01
TOTAL	101.58	100.95	99.47	98.73	98.94	99.06	99.57	98.15	98.14
			Cations/24 Oxygens						
Si	6.066	5.997	6.010	6.186	6.305	5.974	6.113	5.969	5.989
Al	3.571	3.620	3.705	3.568	3.419	3.785	3.442	3.707	3.642
Ti	0.047	0.056	0.080	0.089	0.100	0.105	0.105	0.096	0.136
Fe	1.860	1.750	2.078	1.531	1.556	1.860	1.754	1.776	1.736
Mg	2.731	2.939	2.489	3.319	3.130	2.987	2.990	3.035	3.190
Mn	0.116	0.184	0.084	0.078	0.089	0.072	0.060	0.066	0.068
Ca	1.700	1.584	1.602	1.145	1.262	1.236	1.551	1.418	1.262
Na	0.003	-	-	0.035	0.033	0.010	0.076	0.015	0.048
K	0.009	0.005	0.010	0.008	0.003	0.001	0.002	0.003	0.002
Mg/(Mg+ΣFe)	0.59	0.63	0.54	0.68	0.67	0.62	0.63	0.63	0.65

*Total iron as FeO

Table 3. Orthopyroxene compositions

Analysis Rock	1 Andesite	2 Andesite	3 Andesite
$X^V_{H_2O}$	∿ 0.75	∿ 0.50	∿ 0.25
P, Kbar	13	13	13
T,°C	900	940	940
SiO_2	49.56	51.09	49.68
TiO_2	0.46	0.55	0.53
Al_2O_3	1.77	3.49	1.67
FeO*	22.67	22.29	24.75
MgO	22.55	20.72	19.41
MnO	0.61	0.56	0.50
CaO	1.58	1.82	1.74
Na_2O	-	0.26	0.13
K_2O	0.09	0.02	-
TOTAL	99.29	100.80	98.41
	Cations/6 Oxygens		
Si	1.885	1.899	1.921
Ti	0.013	0.015	0.015
Al	0.079	0.153	0.076
Fe	0.721	0.693	0.800
Mg	1.278	1.148	1.119
Mn	0.020	0.018	0.016
Ca	0.064	0.073	0.072
Na	-	0.019	0.010
K	0.004	0.001	-
Mg/(Mg+ΣFe)	0.64	0.62	0.58

*Total iron as FeO.

the basalt is 1050°C, occurring at X^VH_2O of ~0.25 (and 0.50 at 13 kbar). The maximum pressure stability is 20.5 kbar at X^VH_2O of ~1.0 and decreases as the X^VH_2O is decreased.

The position and configuration of the vapor-saturated silicate liquidi are a complex function of the solubility of a complicated clinopyroxene solid solution in an equally complex silicate liquid. Although the slopes and positions of these liquidi of the basalt have been established by reversed experiments (Table 1), at this time we have no explanation for the changes in slope of these curves as a function of fH_2O and fO_2 as shown in Figure 2.

Chemical analyses

The chemical composition of orthopyroxenes, clinopyroxenes, amphiboles, garnets, and glasses were determined with an ETEC electron microprobe analyzer (Tables 2–6). In computing the chemical analyses, the raw counts were corrected using the method of Bence and Albee (1968). An APL program prepared by V. J. Wall used Fe_2O_3/FeO = 0.8 to compute the structural formulae of the amphiboles; this value is not inconsistent with the amphibole analyses in Leake (1968). H_2O in the amphiboles was arbitrarily taken as 2.00 percent when computing the structural formulae with 24 oxygens, to use the classification of Leake; however, the structural formulae in Table 5b were computed assuming 23 oxygens and no H_2O. Salient features of these determinations are as follows:

Garnet. Garnet occurs at high pressures in both the andesite and the basalt. The chemical analyses of these garnets (Table 2) indicate that Mg/(Mg+ΣFe) is generally proportional to that of the starting material, ranging from 0.54 to 0.63 in the andesite and from 0.62 to 0.68 in the basalt. This compares to values of 0.33 to 0.44 for the same rocks under conditions of lower fO_2 (N–NO) (Boettcher *et al.*, 1973) used in our previous investigation (Allen *et al.*, 1975).

Orthopyroxene. Orthopyroxene was synthesized in the andesite only at X^VH_2O ~ 0.75 or less. Although it was found to be fairly abundant at pressures of 10–14 kbar, it diminished to minor or trace amounts above 15 kbar. The Mg/(Mg+ΣFe) of the orthopyroxenes synthesized from the andesite (Table 3) indicates that they are hypersthenes. Orthopyroxene was synthesized in the basalt only at X^VH_2O ~ 0.25, and then only in trace amounts.

Clinopyroxene. Near liquidus temperatures, clinopyroxene is the most abundant mineral in both the andesite and the basalt, regardless of the X^VH_2O. For the andesite, this is in contrast to the products synthesized at N–NO conditions (Allen *et al.*, 1975), when clinopyroxene did not form. The chemistry of these clinopyroxenes (Table 4), which are dominantly augites, indicates that their Mg/(Mg+ΣFe) reflects that of the starting material.

Amphibole. Amphibole is present in only minor amounts near the high-temperature part of the amphibole-out curve, but is increasingly abundant in runs at successively lower temperatures. As is the case with the other minerals, Mg/(Mg+ΣFe) of the amphiboles (Table 5a) reflects the chemistry of the starting materials, although there is some overlap in this case. Otherwise, the amphiboles are all similar in composition, especially in terms of their SiO_2 content and total alkalis. Those synthesized from the andesite are slightly higher in Al_2O_3 and contain less than half as much TiO_2 as the amphiboles synthesized from the basalt. The difference between the Mg/(Mg+ΣFe) of the amphiboles synthesized under M–H conditions (Table 5a) and those synthesized under N–NO conditions (Allen *et al.*, 1975) is similar to that previously described for the garnets.

According to the classification devised by Leake

Table 4. Clinopyroxene compositions

Analysis Rock.	1 Andesite	2 Andesite	3 Basalt	4 Basalt	5 Basalt	6 Basalt	7 Basalt	8 Basalt	9 Basalt
$X^v_{H_2O}$	∿ 0.50	∿ 0.50	∿ 1.0	∿ 1.0	∿ 0.75	∿ 0.75	∿ 0.75	∿ 0.75	∿ 0.50
P, Kbar	13	13	13	13	20	20	18	13	13
T, °C	940	940	960	960	980	980	980	985	1010
SiO_2	50.98	48.29	50.79	52.30	50.32	49.38	49.03	44.47	44.69
TiO_2	0.88	0.61	0.65	0.84	1.59	0.96	0.62	2.25	3.05
Al_2O_3	1.32	2.19	2.78	2.99	6.82	8.58	7.79	8.48	8.01
FeO*	14.50	14.27	5.09	5.34	9.63	7.93	6.89	9.57	10.26
MgO	14.47	13.66	15.70	15.56	13.59	10.80	13.33	13.70	12.56
MnO	0.43	0.35	0.08	0.14	0.20	0.21	0.18	0.22	0.26
CaO	18.48	18.95	23.35	22.94	17.17	19.03	20.84	20.29	19.91
Na_2O	0.36	0.20	0.33	0.30	0.80	1.31	0.88	0.60	0.62
K_2O	-	0.01	0.02	0.02	0.06	0.02	-	0.02	-
TOTAL	101.42	98.53	98.79	100.43	100.18	98.22	99.56	99.60	99.36
				Cations/6 Oxygens					
Si	1.914	1.876	1.897	1.916	1.854	1.852	1.818	1.685	1.702
Al	0.058	0.100	0.122	0.129	0.296	0.379	0.340	0.379	0.360
Ti	0.025	0.018	0.018	0.023	0.044	0.027	0.017	0.064	0.087
Fe	0.455	0.464	0.159	0.164	0.297	0.249	0.213	0.303	0.327
Mg	0.810	0.791	0.874	0.849	0.747	0.604	0.737	0.774	0.713
Mn	0.014	0.012	0.002	0.004	0.006	0.007	0.005	0.006	0.008
Ca	0.743	0.789	0.935	0.900	0.678	0.765	0.828	0.824	0.812
Na	0.026	0.015	0.023	0.021	0.057	0.095	0.063	0.044	0.046
K	-	-	0.001	0.001	0.003	0.001	-	-	-
$\frac{Mg}{(Mg+\Sigma Fe)}$	0.64	0.63	0.84	0.84	0.72	0.71	0.78	0.72	0.69
Mg	40.3	38.7	44.4	44.4	43.4	37.3	41.4	40.7	38.5
Fe	22.7	22.7	8.1	8.6	17.2	15.4	12.0	15.9	17.7
Ca	37.0	38.6	47.5	47.0	39.4	47.3	46.6	43.4	43.8

*Total iron as FeO

(1968), these amphiboles straddle the calciferous–subcalciferous boundary, although most are calciferous as well as tschermakitic. Only seven, all synthesized from the basalt, contain enough titanium to justify the prefix titaniferous (0.25 Ti per 24 oxygens). The amphiboles for which we have data, synthesized from the andesite, become less magnesian with increasing pressure at $X^VH_2O \sim 1.0$, similar to the trend found by Mysen and Boettcher (1975) for amphibole in peridotite at high pressures; however, the amphiboles synthesized from the basalt show no apparent trend in this regard. All but two of the amphiboles (Table 5c) are nepheline-normative.

Glasses. Representative chemical analyses of glasses produced from the andesite and basalt are listed in Table 6. Analyses of glasses have been normalized to 100 percent because of their large and variable H_2O contents. The total Fe was distributed between FeO and Fe_2O_3 according to the scheme described above for the amphiboles. The glasses formed from the andesite are higher in SiO_2 than those from the basalt. All the glasses are high in Al_2O_3 and CaO and are quartz-normative. All but one of the glasses contain less Na_2O than the coexisting amphiboles. Note that the glasses formed from the andesite at $X^VH_2O \sim 0.25$ have significantly higher Na_2O than the other glasses, reflecting the fact that amphibole is not stable under these conditions. All but two of the glasses contain more K_2O than their associated amphiboles.

In Table 6a, the discrepancy between analyses 1 and 2 may result from inclusions of opaque material in the glass. In addition, some gradients in MgO and FeO occur in glasses within ~30 μm of amphiboles.

Table 4. (continued)

Analysis	10	11	12	13	14	15	16	17	18
Rock	Basalt	Basalt	Basalt	Basalt	Basalt	Basalt	Basalt	Basalt	Basalt
$X^v_{H_2O}$	∿ 0.50	∿ 0.50	∿ 0.50	∿ 0.50	∿ 0.50	∿ 0.50	∿ 0.25	∿ 0.25	∿ 0.25
P, Kbar	13	13	13	13	21	21	13	13	13
T, °C	1010	1010	1010	1010	1020	1020	1025	1025	1025
SiO_2	43.98	44.09	48.35	46.96	50.15	48.84	49.00	48.98	50.40
TiO_2	3.22	2.84	1.05	2.02	1.57	0.75	1.36	1.00	1.52
Al_2O_3	8.29	10.17	6.52	7.27	9.43	10.50	5.05	6.50	4.73
FeO*	10.32	9.47	7.21	8.65	9.73	8.56	9.81	9.06	10.89
MgO	12.60	12.73	14.61	14.24	9.70	11.34	16.79	15.90	14.76
MnO	0.23	0.21	0.22	0.27	0.18	0.06	0.20	0.20	0.17
CaO	20.42	20.24	21.27	20.23	16.08	18.05	18.58	19.16	18.75
Na_2O	0.61	0.72	0.58	0.57	1.64	2.06	0.63	0.64	0.46
K_2O	0.01	0.04	0.02	0.02	0.19	0.01	0.04	0.01	0.01
TOTAL	99.68	100.51	99.83	100.23	98.67	100.17	101.46	101.45	101.69
				Cations/6 Oxygens					
Si	1.674	1.653	1.799	1.752	1.868	1.799	1.805	1.797	1.853
Al	0.372	0.449	0.286	0.320	0.414	0.456	0.219	0.281	0.205
Ti	0.092	0.080	0.029	0.056	0.044	0.021	0.038	0.028	0.042
Fe	0.328	0.297	0.224	0.270	0.303	0.264	0.302	0.278	0.335
Mg	0.715	0.711	0.811	0.792	0.539	0.623	0.922	0.869	0.809
Mn	0.007	0.006	0.006	0.008	0.006	0.002	0.006	0.006	0.005
Ca	0.833	0.814	0.848	0.809	0.642	0.713	0.733	0.753	0.738
Na	0.045	0.052	0.041	0.040	0.119	0.147	0.045	0.046	0.033
K	-	0.002	-	0.001	0.009	-	0.002	-	-
$\frac{Mg}{(Mg+\Sigma Fe)}$	0.69	0.71	0.78	0.75	0.64	0.70	0.75	0.76	0.71
Mg	38.1	39.0	43.1	42.3	36.3	38.9	47.1	45.7	43.0
Fe	17.5	16.3	11.9	14.4	20.4	16.5	15.4	14.6	17.8
Ca	44.4	44.7	45.0	43.3	43.3	44.6	37.5	39.7	39.2

*Total iron as FeO .

Discussion

Reducing X^vH_2O does not change the basic configuration of the amphibole-out curves in the andesite and basalt melts as compared to our studies carried out in the presence of nearly pure H_2O (Allen *et al.*, 1975). However, varying X^vH_2O does bring about a change in the location of the stability fields of the amphiboles, and in the case of the andesite, if X^vH_2O is reduced below ~0.25, amphibole is not stable above the solidus. The thermal stability of amphibole is increased somewhat by lowering X^vH_2O below 1.0, although in the case of the andesite, this initial increase in stability is reversed when X^vH_2O is decreased below ~0.75. This increase in the stability of amphiboles brings about an increase in the depth at which the amphibole-out curves would intersect an oceanic geotherm, although this increase would only amount to a kilometer or two. The fact that amphiboles are not stable in andesite with X^vH_2O ~0.25, but do occur in some andesites, indicates that aH_2O must be fairly high at least in the later stages of the ascent of some magmas in volcanic conduits, a conclusion reached by Anderson (1974).

These results are consistent with the results of our earlier study in that the amphiboles in the basalt are stable to temperatures greater than the vapor-saturated liquidus of the andesite, except at $X^vH_2O \lesssim 0.25$, in which case amphibole is absent above the andesite solidus. Separation of these low-silica amphiboles (41.5 to 45.0 percent SiO_2) from basaltic magmas by fractional crystallization or partial melting in the presence of water would be an effective process leading toward silica enrichment of the liquid, as proposed by Bowen (1928, p. 85–91) and applied to derivations of andesitic magmas in subduction zones by Boettcher (1977). Our data are, of course, only directly applicable to amphibole fractionation at high pressures, *i.e.*, above 10 kbar, and they do not rule out amphibole fractionation as an effective process in the generation of andesites at lower pressures as suggested by Cawthorn and

Table 5a. Amphibole compositions

Analysis	1	2	3	4	5	6	7	8	9	10	11
Rock					Andesite						
$X^v_{H_2O}$	∿ 1.0	∿ 1.0	∿ 1.0	∿ 1.0	∿ 1.0	∿ 1.0	∿ 1.0	∿ 1.0	∿ 1.0	∿ 0.75	∿ 0.75
P, Kbar	13	13	13	17	17	17	17	17	17	13	13
T, °C	920	920	920	920	920	920	920	920	920	900	900
SiO_2	44.74	45.60	45.05	45.16	44.30	44.41	43.18	42.66	44.49	41.72	44.06
TiO_2	0.73	0.51	0.55	0.81	0.46	0.16	0.36	0.47	0.33	0.49	0.70
Al_2O_3	13.64	12.88	13.34	11.71	14.07	14.33	16.75	17.41	14.27	17.10	12.78
Fe_2O_3*	3.69	3.66	3.70	5.83	4.53	5.01	5.43	5.28	4.86	5.01	6.35
FeO	4.62	4.57	4.63	7.29	5.66	6.27	6.79	6.60	6.08	6.27	7.94
MgO	16.61	16.69	16.23	13.62	15.24	15.63	12.86	13.25	14.74	14.47	16.53
MnO	0.10	0.19	0.19	0.26	0.12	0.12	0.16	0.19	0.26	0.23	0.27
CaO	11.30	11.17	11.14	10.67	11.90	11.27	11.39	11.23	11.81	10.03	7.17
Na_2O	2.31	1.87	1.80	1.66	2.24	2.31	2.08	2.27	2.41	2.26	1.62
K_2O	0.31	0.33	0.34	0.41	0.48	0.44	0.46	0.44	0.47	0.57	0.39
H_2O*	2.00	2.00	2.00	2.00	2.00	2.00	2.00	2.00	2.00	2.00	2.00
TOTAL	100.05	99.47	98.97	99.42	101.00	101.95	101.46	101.80	101.72	100.15	99.81
$\frac{Mg}{(Mg+\Sigma Fe)}$	0.79	0.79	0.78	0.66	0.74	0.72	0.66	0.68	0.72	0.71	0.68
$\frac{Mg}{(Mg+Fe^{2+})}$	0.86	0.87	0.86	0.77	0.83	0.82	0.77	0.78	0.81	0.80	0.79

Estimate, See Text.

Analysis	12	13	14	15	16	17	18	19	20	21
Rock					Andesite					
$X^v_{H_2O}$	∿ 0.75	∿ 0.75	∿ 0.75	∿ 0.50	∿ 0.50	∿ 0.50	∿ 0.50	∿ 0.50	∿ 0.50	∿ 0.50
P, Kbar	13	13	13	13	13	13	13	13	13	13
T, °C	900	900	900	925	925	925	925	925	940	940
SiO_2	40.63	41.13	41.27	41.28	43.43	43.04	41.73	41.24	40.47	41.41
TiO_2	0.62	0.93	0.70	1.40	1.56	1.03	1.33	1.03	0.83	1.11
Al_2O_3	17.54	16.31	15.72	16.03	17.15	17.09	17.37	16.10	15.25	14.61
Fe_2O_3*	4.96	5.78	4.33	4.22	4.00	4.04	4.54	4.46	5.50	5.49
FeO	6.20	7.23	5.42	5.28	5.01	5.05	5.67	5.58	6.88	6.87
MgO	14.02	14.14	16.98	16.33	15.31	16.06	15.08	17.63	14.69	14.65
MnO	0.18	0.21	0.23	0.24	0.24	0.15	0.21	0.27	0.14	0.21
CaO	10.20	9.60	11.02	10.50	10.03	9.29	10.72	11.04	11.12	10.18
Na_2O	2.43	2.62	2.11	2.42	2.42	2.24	2.49	2.40	2.00	2.04
K_2O	0.48	0.46	0.56	0.38	0.43	0.43	0.44	0.37	0.40	0.47
H_2O*	2.00	2.00	2.00	2.00	2.00	2.00	2.00	2.00	2.00	2.00
TOTAL	99.26	100.41	100.34	100.08	101.58	100.42	101.58	102.12	99.28	99.05
$\frac{Mg}{(Mg+\Sigma Fe)}$	0.70	0.67	0.76	0.76	0.76	0.77	0.73	0.77	0.69	0.69
$\frac{Mg}{(Mg+Fe^{2+})}$	0.80	0.78	0.85	0.85	0.84	0.85	0.83	0.85	0.79	0.79

Estimate, See Text.

Table 5a. (continued)

Analysis	22	23	24	25	26	27	28	29	30
Rock	Basalt	Basalt	Basalt	Basalt	Basalt	Basalt	Basalt	Basalt	Basalt
$X^v_{H_2O}$	∿ 1.0	∿ 0.75	∿ 0.75	∿ 0.75	∿ 0.75	∿ 0.75	∿ 0.75	∿ 0.50	∿ 0.50
P, Kbar	13	13	13	18	18	18	18	13	13
T, °C	960	985	985	980	980	980	980	1010	1010
SiO_2	45.00	43.67	42.06	44.93	44.79	43.97	43.92	41.70	43.68
TiO_2	1.37	2.08	2.26	1.04	0.88	1.07	0.99	2.87	1.65
Al_2O_3	12.27	11.93	13.28	14.43	15.09	14.73	14.95	13.18	12.60
Fe_2O_3*	3.04	3.94	3.98	3.42	3.35	3.08	3.58	4.31	3.57
FeO	3.81	4.93	4.98	4.27	4.19	3.84	4.48	5.39	4.46
MgO	17.69	18.02	17.46	16.96	18.15	17.04	14.87	15.84	17.75
MnO	0.19	0.31	0.14	0.19	0.10	0.09	0.13	0.16	0.20
CaO	11.41	10.55	11.26	10.68	10.91	11.19	11.98	11.18	11.30
Na_2O	2.00	2.11	2.32	1.93	1.88	2.00	2.06	1.89	1.59
K_2O	0.38	0.36	0.45	0.69	0.61	0.72	0.59	0.59	0.53
H_2O*	2.00	2.00	2.00	2.00	2.00	2.00	2.00	2.00	2.00
TOTAL	99.16	99.90	100.19	100.54	101.95	99.73	99.55	99.11	99.33
$\frac{Mg}{(Mg+\Sigma Fe)}$	0.83	0.79	0.78	0.80	0.82	0.82	0.77	0.75	0.80
$\frac{Mg}{(Mg+Fe^{2+})}$	0.89	0.87	0.86	0.88	0.89	0.89	0.85	0.84	0.88

Estimate, See Text.

Analysis	31	32	33	34	35	36	37	38	39
Rock	Basalt	Basalt	Basalt	Basalt	Basalt	Basalt	Basalt	Basalt	Basalt
$X^v_{H_2O}$	∿ 0.50	∿ 0.50	∿ 0.50	∿ 0.50	∿ 0.50	∿ 0.25	∿ 0.25	∿ 0.25	∿ 0.25
P, Kbar	13	13	13	13	13	13	13	13	13
T, °C	1010	1010	1010	1010	1010	1025	1025	1025	1025
SiO_2	42.80	42.34	42.48	41.96	43.60	42.06	41.63	43.75	41.52
TiO_2	1.68	2.68	1.94	2.79	1.80	2.44	2.56	2.36	2.42
Al_2O_3	13.22	12.42	12.82	13.30	12.97	15.47	15.91	16.58	17.02
Fe_2O_3*	3.51	4.28	3.63	4.44	3.60	4.46	4.71	4.24	4.65
FeO	4.39	5.35	4.54	5.54	4.49	5.57	5.89	5.29	5.81
MgO	17.99	16.03	17.20	16.23	17.00	16.03	14.91	13.57	14.71
MnO	0.12	0.09	0.16	0.13	0.26	0.11	0.10	0.22	0.16
CaO	11.42	12.04	12.40	11.41	11.31	10.39	9.99	9.87	10.45
Na_2O	1.80	1.65	1.82	1.79	1.65	1.94	1.95	1.76	1.90
K_2O	0.59	0.57	0.59	0.68	0.59	0.92	1.12	1.30	1.22
H_2O*	2.00	2.00	2.00	2.00	2.00	2.00	2.00	2.00	2.00
TOTAL	99.52	99.45	99.58	100.27	99.27	101.39	100.77	100.94	101.86
$\frac{Mg}{(Mg+\Sigma Fe)}$	0.81	0.76	0.80	0.75	0.80	0.75	0.72	0.73	0.72
$\frac{Mg}{(Mg+Fe^{2+})}$	0.88	0.84	0.87	0.84	0.87	0.84	0.82	0.82	0.82

Estimate, See Text.

Table 5b. Chemical formulae (0–23) for amphiboles in Table 5a

Formula	1	2	3	4	5	6	7	8	9	10	11
Si	6.348	6.485	6.443	6.543	6.287	6.225	6.125	6.030	6.287	5.983	6.336
Al^{IV}	1.652	1.515	1.557	1.457	1.713	1.775	1.875	1.970	1.713	2.017	1.664
Al^{VI}	0.631	0.646	0.693	0.544	0.642	0.606	0.928	0.933	0.666	0.876	0.504
Ti	0.078	0.055	0.059	0.088	0.049	0.017	0.038	0.050	0.035	0.053	0.076
Fe^{3+}	0.394	0.392	0.398	0.636	0.484	0.531	0.580	0.562	0.517	0.541	0.687
Mg	3.512	3.538	3.459	2.941	3.223	3.281	2.719	2.791	3.104	3.093	3.543
Fe^{2+}	0.548	0.544	0.554	0.883	0.672	0.738	0.806	0.780	0.719	0.752	0.955
Mn	0.012	0.023	0.023	0.032	0.014	0.014	0.019	0.023	0.031	0.028	0.033
Ca	1.718	1.702	1.707	1.657	1.810	1.701	1.731	1.701	1.788	1.541	1.105
Na	0.635	0.516	0.499	0.466	0.616	0.631	0.572	0.622	0.660	0.628	0.452
K	0.056	0.060	0.062	0.076	0.087	0.079	0.083	0.079	0.085	0.104	0.072
Ca+Na+K	2.409	2.278	2.268	2.199	2.513	2.411	2.386	2.402	2.533	2.273	1.629
mg	0.79	0.79	0.78	0.65	0.73	0.72	0.66	0.67	0.71	0.70	0.68
Classification*	t.h.	t.h.	t.h.	m.h.	f.p.h.	t.h.	t.	t.	f.p.h.	t.	t.h.
Fe/Mg	0.27	0.26	0.28	0.52	0.36	0.39	0.51	0.48	0.40	0.42	0.46

Formula	12	13	14	15	16	17	18	19	20	21	22
Si	5.891	5.933	5.913	5.913	6.068	6.070	5.893	5.816	5.920	6.049	6.416
Al^{IV}	2.109	2.067	2.087	2.087	1.932	1.930	2.107	2.184	2.080	1.951	1.584
Al^{VI}	0.891	0.708	0.570	0.621	0.894	0.913	0.786	0.494	0.551	0.566	0.480
Ti	0.068	0.101	0.075	0.151	0.164	0.109	0.141	0.109	0.091	0.122	0.147
Fe^{3+}	0.541	0.628	0.467	0.455	0.421	0.429	0.483	0.474	0.606	0.604	0.326
Mg	3.030	3.040	3.626	3.486	3.188	3.375	3.174	3.705	3.202	3.189	3.759
Fe^{2+}	0.752	0.872	0.649	0.633	0.585	0.596	0.670	0.658	0.842	0.839	0.454
Mn	0.022	0.026	0.028	0.029	0.028	0.018	0.025	0.032	0.017	0.026	0.023
Ca	1.585	1.484	1.692	1.612	1.502	1.404	1.622	1.668	1.743	1.593	1.743
Na	0.683	0.733	0.586	0.672	0.656	0.612	0.682	0.656	0.567	0.578	0.553
K	0.089	0.085	0.102	0.069	0.077	0.077	0.079	0.067	0.075	0.088	0.069
Ca+Na+K	2.357	2.302	2.380	2.353	2.235	2.093	2.383	2.391	2.385	2.259	2.365
mg	0.70	0.67	0.76	0.76	0.76	0.76	0.73	0.76	0.69	0.69	0.82
Classification*	t.	t.	t.	t.	t.	t.	t.	t.	t.	t.	t.h.
Fe/Mg	0.43	0.49	0.31	0.31	0.32	0.30	0.36	0.31	0.45	0.45	0.21

Formula	23	24	25	26	27	28	29	30	31	32	33
Si	6.245	6.031	6.318	6.209	6.237	6.273	6.058	6.260	6.137	6.132	6.120
Al^{IV}	1.755	1.969	1.682	1.791	1.763	1.727	1.942	1.740	1.863	1.868	1.880
Al^{VI}	0.257	0.277	0.711	0.676	0.702	0.792	0.316	0.390	0.373	0.254	0.299
Ti	0.224	0.244	0.110	0.092	0.114	0.106	0.314	0.178	0.181	0.292	0.210
Fe^{3+}	0.424	0.430	0.362	0.350	0.329	0.385	0.471	0.385	0.379	0.467	0.394
Mg	3.841	3.731	3.554	3.750	3.602	3.165	3.429	3.791	3.844	3.460	3.693
Fe^{2+}	0.590	0.597	0.502	0.486	0.456	0.535	0.655	0.535	0.526	0.648	0.547
Mn	0.038	0.017	0.023	0.012	0.011	0.016	0.020	0.024	0.015	0.011	0.020
Ca	1.617	1.730	1.609	1.621	1.701	1.833	1.740	1.735	1.755	1.868	1.914
Na	0.585	0.645	0.526	0.505	0.550	0.570	0.532	0.442	0.500	0.463	0.508
K	0.066	0.082	0.124	0.108	0.130	0.108	0.109	0.097	0.108	0.105	0.108
Ca+Na+K	2.268	2.457	2.259	2.234	2.381	2.511	2.381	2.274	2.363	2.436	2.530
mg	0.78	0.78	0.80	0.82	0.82	0.77	0.75	0.80	0.81	0.75	0.79
Classification*	t.h.	t.	t.h.	t.	t.h.	p.h.	t.	t.h.	t.	t.	p.
Fe/Mg	0.26	0.28	0.24	0.22	0.22	0.29	0.33	0.24	0.24	0.32	0.25

Table 5b. (continued)

Formula	34	35	36	37	38	39
Si	6.033	6.255	5.956	5.943	6.170	5.867
Al^{IV}	1.967	1.745	2.044	2.057	1.830	2.133
Al^{VI}	0.289	0.450	0.540	0.622	0.928	0.704
Ti	0.302	0.194	0.260	0.275	0.250	0.257
Fe^{3+}	0.481	0.389	0.476	0.506	0.450	0.495
Mg	3.478	3.635	3.383	3.172	2.852	3.098
Fe^{2+}	0.666	0.539	0.660	0.703	0.624	0.687
Mn	0.016	0.032	0.013	0.012	0.026	0.019
Ca	1.758	1.739	1.577	1.528	1.491	1.582
Na	0.499	0.459	0.533	0.540	0.481	0.521
K	0.125	0.108	0.166	0.204	0.234	0.220
Ca+Na+K	2.382	2.306	2.276	2.272	2.206	2.323
mg	0.75	0.79	0.75	0.72	0.72	0.72
Classification*	t.	t.h.	t.	t.	t.	t.
Fe/Mg	0.33	0.25	0.34	0.38	0.38	0.38

p. = *pargasite; t.* = *tschermakite; p.h.* = *pargasitic hornblende; t.h.* - *tschermakitic hornblende; f.p.h.* = *ferroan pargasitic hornblende; m.h.* = *magnesio-hornblende*

**On the basis of 24 oxygens, according to classification of Leake (1968)*

O'Hara (1976). However, the conversion of amphibole-bearing assemblages to garnet-bearing assemblages at higher pressures (Figs. 1 and 2) does set a depth limit on the viability of amphibole-liquid equilibria in the generation of andesitic magma.

Our model is consistent with the abundances of Sc, Cr, Ni, and probably Co in andesites in Chile (Lopez-Escobar *et al.*, 1976); it is also rather consistent with similar data for K, Rb, Sr, and Ba if altered basalt is considered (Lopez-Escobar *et al.*, 1976; Frey *et al.*, 1974; Hart, 1969). However, this model is not consistent with calculated REE and especially HREE abundances (Lopez-Escobar *et al.*, 1976; Thorpe *et al.*, 1976). This supposed lack of consistency may be more apparent than real, for the experimental partition coefficients for REE between amphibole/liquid have been criticized on the basis of (1) possible imperfect phase separation for analysis, (2) failure to achieve and demonstrate equilibrium, and (3) continued and variable loss of Fe to the noble-metal capsules during experimentation with Fe-bearing natural rock assemblages. Apted *et al.* (1977) are currently conducting experiments to obtain data free of such criticisms.

Ringwood (1974) states that amphibole fractionation would not "produce the tholeiite early iron-enrichment trend," for the Fe/Mg of amphibole is comparable to the Fe/Mg of the magma. However, the Fe/Mg data in Table 5 do not support Ringwood's thesis; this ratio for each of the amphiboles in Table 5 is lower than that of the starting material. Thus these data are in agreement with our earlier data (Allen *et al.*, 1975), and fractionation of these amphiboles over a range of fO_2 and fH_2O could very well contribute to the tholeiitic trend of early iron enrichment. Ringwood also states that amphibole fractionation would not "greatly alter Na/K ratio of residual liquid or partial melt" because Na/K of amphiboles and the liquids from which they crystallize are comparable. Comparison of Na/K of the synthesized amphiboles (Table 5) and their parent basalt reveals that almost all of the amphiboles have a lower Na/K than the basalt; the reverse is true for the andesite.

Applications of our experimental investigations of the phase relationships of andesites and basalts to volcanism in orogenic zones have been aired previously (Boettcher, 1973, 1977; Allen *et al.*, 1975). Our basic proposal is that amphiboles are a major carrier of H_2O in subducted oceanic slabs and that crystal-liquid equilibria involving amphiboles are prominent in the genesis of calc-alkaline magmas. This model has been criticized, because Benioff zones are commonly assumed to dip at 45° or greater, and because melting is assumed to occur along these seismic zones. This places the depth of magma genesis at 150–250 km beneath active volcanic chains—much greater than the depth to which amphiboles are stable under any known conditions. However, the dip of downgoing slabs is commonly much shallower than 45° at oceanic-continental plate boundaries. In addition the zones of magma genesis are probably at shallower depths, at the tops of the slabs, whereas the seismic zones coincide with the cooler interior of the slab where brittle, not plastic, behavior prevails (Boettcher, 1977).

Recent data that can be interpreted in support of this model are those of Barazangi and Isacks (1976) for the west coast of South America. Their compilation of hypocenters reveals that the oceanic plate descending beneath the continent is divided into five segments. Three of these segments (0°–2°S, 15°–27°S, and 33°–45°S) have dips on the order of 25° to 30° and are regions of well-developed Quaternary volcanism. The intervening segments (2°–15°S and 27°–33°S) have dips of about 10°, exhibit no high attenuation of seismic waves in the underlying mantle, and are devoid of Quarternary volcanism.

Barazangi and Isacks ascribed the correlation of dip and volcanic activity to the apparent absence of "asthenospheric material" between the descending slab and the continental plate in the two regions overlying the flat-lying slabs. An alternative explanation is that in the three regions with dips of 25°–

Table 5c. Normative compositions (C.I.P.W.) of amphiboles in Table 5a

Norm	1	2	3	4	5	6	7	8	9	10
orthoclase	1.83	1.95	2.01	2.42	2.84	2.60	2.72	2.60	2.78	3.37
albite	10.32	14.02	13.52	14.05	7.28	8.41	8.65	6.75	7.75	6.33
anorthite	25.94	25.78	27.32	23.29	26.92	27.43	35.01	36.02	26.73	34.83
nepheline	5.00	0.98	0.93	-	6.32	6.03	4.85	6.75	6.85	6.93
leucite	-	-	-	-	-	-	-	-	-	-
diopside	23.71	23.35	22.03	23.57	25.40	22.57	17.11	15.65	25.26	11.84
wo	(12.58)	(12.38)	(11.67)	(12.38)	(13.41)	(11.89)	(8.98)	(8.22)	(13.30)	(6.23)
en	(10.06)	(9.82)	(9.24)	(9.12)	(10.33)	(8.99)	(6.56)	(6.08)	(10.02)	(4.70)
fs	(1.07)	(1.15)	(1.12)	(2.08)	(1.66)	(1.69)	(1.57)	(1.35)	(1.94)	(0.91)
hypersthene	-	-	-	8.27	-	-	-	-	-	-
en	-	-	-	(6.74)	-	-	-	-	-	-
fs	-	-	-	(1.53)	-	-	-	-	-	-
olivine	24.52	25.12	24.77	15.83	22.80	25.33	22.57	23.48	22.68	26.66
fo	(21.94)	(22.24)	(21.85)	(12.66)	(19.36)	(20.98)	(17.84)	(18.86)	(18.70)	(21.96)
fa	(2.58)	(2.88)	(2.92)	(3.17)	(3.42)	(4.35)	(4.72)	(4.62)	(3.98)	(4.70)
magnetite	5.35	5.31	5.37	8.45	6.57	7.26	7.87	7.66	7.05	7.26
ilmenite	1.39	0.97	1.05	1.54	0.87	0.30	0.68	0.89	0.63	0.93

Norm	11	12	13	14	15	16	17	18	19	20
orthoclase	2.31	2.84	2.72	3.10	2.25	2.54	2.54	2.60	0.36	2.36
albite	13.71	4.15	7.11	-	3.64	10.83	11.59	4.09	-	2.74
anorthite	26.45	35.54	31.39	31.77	31.76	34.67	35.31	34.92	32.07	31.45
nepheline	-	8.89	8.16	9.67	9.12	5.23	3.99	9.20	11.00	7.68
leucite	-	-	-	0.17	-	-	-	-	1.44	-
diopside	7.24	11.94	12.90	18.07	16.00	11.87	8.49	14.40	17.89	18.80
wo	(3.81)	(6.29)	(6.78)	(9.56)	(8.49)	(6.30)	(4.50)	(7.62)	(9.48)	(9.90)
en	(2.83)	(4.75)	(5.06)	(7.51)	(6.79)	(5.07)	(3.58)	(6.00)	(7.50)	(7.47)
fs	(0.60)	(0.90)	(1.06)	(1.00)	(0.72)	(0.50)	(0.41)	(0.78)	(0.91)	(1.43)
hypersthene	15.58	-	-	-	-	-	-	-	-	-
en	(12.87)	-	-	-	-	-	-	-	-	-
fs	(2.71)	-	-	-	-	-	-	-	-	-
olivine	21.99	25.54	26.00	27.96	26.54	25.69	28.69	25.26	28.95	24.69
fo	(17.84)	(21.14)	(21.13)	(24.37)	(23.74)	(23.17)	(25.52)	(22.11)	(25.51)	(20.40)
fa	(4.15)	(4.40)	(4.87)	(3.59)	(2.80)	(2.52)	(3.17)	(3.15)	(3.44)	(4.29)
magnetite	9.21	7.19	8.38	6.28	6.12	5.80	5.86	6.58	6.47	7.97
ilmenite	1.33	1.18	1.77	1.33	2.66	2.96	1.96	2.53	1.96	1.58

Norm	21	22	23	24	25	26	27	28	29	30
orthoclase	2.78	2.25	2.13	2.66	4.08	3.61	4.26	3.49	3.49	3.13
albite	8.07	10.99	10.41	3.37	10.51	7.80	6.22	7.05	6.10	8.18
anorthite	29.32	23.38	22.02	24.49	28.67	30.94	29.09	29.81	25.74	25.68
nepheline	4.98	3.22	4.04	8.81	3.16	4.39	5.80	5.62	5.36	2.86
leucite	-	-	-	-	-	-	-	-	-	-
diopside	16.78	26.02	23.77	24.56	19.10	18.21	20.72	23.31	23.26	23.81
wo	(8.85)	(13.87)	(12.66)	(13.10)	(10.15)	(9.68)	(11.04)	(12.37)	(12.41)	(12.69)
en	(6.71)	(11.48)	(10.43)	(10.87)	(8.24)	(7.89)	(9.06)	(9.90)	(10.35)	(10.44)
fs	(1.22)	(0.67)	(0.68)	(0.60)	(0.71)	(0.64)	(0.62)	(1.04)	(0.50)	(0.68)
hypersthene	-	-	-	-	-	-	-	-	-	-
en	-	-	-	-	-	-	-	-	-	-
fs	-	-	-	-	-	-	-	-	-	-
olivine	25.04	24.30	25.89	24.24	26.10	28.48	25.15	21.20	21.47	25.36
fo	(20.86)	(22.83)	(24.15)	(22.86)	(23.83)	(26.15)	(23.39)	(19.01)	(20.39)	(23.66)
fa	(4.18)	(1.47)	(1.74)	(1.38)	(2.27)	(2.33)	(1.76)	(2.19)	(1.08)	(1.70)
magnetite	7.96	4.41	5.71	5.77	4.96	4.86	4.47	5.19	6.25	5.18
ilmenite	2.11	2.60	3.95	4.29	1.98	1.67	2.03	1.88	5.45	3.13

Table 5c. (continued)

Norm	31	32	33	34	35	36	37	38	39
orthoclase	3.49	3.37	3.49	4.02	3.49	5.44	6.62	7.68	7.21
albite	4.06	5.50	1.50	4.65	8.36	4.78	5.14	11.23	2.16
anorthite	26.25	24.80	25.07	26.25	26.24	30.79	31.35	33.50	34.31
nepheline	6.05	4.58	7.53	5.69	3.04	6.31	6.16	1.98	7.54
leucite	-	-	-	-	-	-	-	-	-
diopside	23.82	27.34	28.54	23.77	23.41	16.28	14.29	12.14	13.77
wo	(12.70)	(14.58)	(15.22)	(12.68)	(12.47)	(8.67)	(7.60)	(6.46)	(7.32)
en	(10.51)	(12.14)	(12.61)	(10.53)	(10.27)	(7.12)	(6.21)	(5.26)	(5.94)
fs	(0.61)	(0.62)	(0.71)	(0.56)	(0.67)	(0.49)	(0.48)	(0.42)	(0.51)
hypersthene	-	-	-	-	-	-	-	-	-
en	-	-	-	-	-	-	-	-	-
fs	-	-	-	-	-	-	-	-	-
olivine	25.58	20.56	22.51	22.17	24.10	24.71	23.53	21.77	23.53
fo	(24.03)	(19.47)	(21.18)	(20.95)	(22.47)	(22.98)	(21.67)	(20.00)	(21.51)
fa	(1.55)	(1.09)	(1.33)	(1.22)	(1.63)	(1.73)	(1.86)	(1.77)	(2.02)
magnetite	5.09	6.21	5.26	6.44	5.22	6.47	6.83	6.15	6.74
ilmenite	3.19	5.09	3.69	5.30	3.42	4.63	4.86	4.48	4.60

Table 6a. Composition of quenched liquids (glass)

Analyses	1	2	3	4	5	6	7	8	9	10	11	12
Rock†	A	A	A	A	A	A	A	A	A	A	A	A
$X^V_{H_2O}$	∿1.0	∿1.0	∿1.0	∿0.75	∿0.75	∿0.75	∿0.75	∿0.75	∿0.75	∿0.5	∿0.5	∿0.5
P, Kbar	13	13	22	13	13	13	13	22	22	13	13	13
T, °C	920	920	920	900	900	900	900	940	940	925	925	925
SiO_2	68.3	63.1	71.3	68.2	69.3	68.2	68.4	67.4	68.7	66.3	67.0	71.2
TiO_2	0.2	0.4	0.0	0.1	0.1	0.1	0.1	0.4	0.7	0.2	0.2	0.3
Al_2O_3	21.4	20.2	19.7	22.1	20.8	21.5	21.3	20.0	19.9	23.5	22.2	19.6
Fe_2O_3*	0.8	2.0	0.4	0.7	0.7	0.9	0.9	1.4	1.3	0.8	0.8	1.0
FeO	1.0	2.5	0.5	0.9	0.9	1.1	1.1	1.8	1.7	1.0	0.9	1.2
MgO	0.5	4.6	-	0.9	0.9	1.6	1.7	1.7	1.7	0.9	1.4	1.0
MnO	0.1	0.3	-	-	0.0	-	-	-	-	0.1	-	0.0
CaO	6.6	5.5	6.0	5.8	6.0	5.4	5.3	5.7	4.1	5.3	5.8	5.2
Na_2O	0.7	0.8	1.5	0.8	0.7	0.7	0.6	0.7	0.7	1.1	1.0	0.2
K_2O	0.2	0.7	0.6	0.6	0.6	0.6	0.5	0.9	1.3	0.7	0.7	0.3
TOTAL	99.8	100.1	100.0	100.1	100.0	100.1	99.9	100.0	100.1	99.9	100.0	100.0
Mg/(Mg+ΣFe)	0.32	0.64	-	0.52	0.49	0.61	0.61	0.49	0.51	0.48	0.60	0.44

Analyses	13	14	15	16	17	18	19	20	21	22	23	24
Rock†	A	A	A	A	A	B	B	B	B	B	B	B
$X^V_{H_2O}$	∿0.5	∿0.5	∿0.25	∿0.25	∿0.25	∿1.0	∿0.75	∿0.75	∿0.50	∿0.50	∿0.25	∿0.25
P, Kbar	13	13	13	13	13	13	18	13	13	13	13	13
T, °C	925	940	940	940	940	960	980	985	1010	1010	1025	1025
SiO_2	70.3	71.7	57.1	61.3	64.0	62.8	61.8	66.6	59.5	60.4	66.2	65.5
TiO_2	0.4	0.4	-	0.1	0.1	0.8	0.7	0.6	1.2	1.3	1.2	1.0
Al_2O_3	18.3	16.1	23.9	23.1	21.1	23.1	19.0	20.8	20.2	20.7	20.4	19.6
Fe_2O_3*	1.3	1.4	0.3	0.4	0.4	1.0	1.6	1.0	2.1	2.1	1.5	1.7
FeO	1.6	1.8	0.4	0.5	0.6	1.2	2.0	1.3	2.6	2.6	1.9	2.1
MgO	1.1	1.8	0.1	0.1	0.3	0.9	3.3	1.6	5.0	3.6	1.6	2.4
MnO	0.2	-	-	-	-	-	0.0	-	0.1	0.1	-	0.0
CaO	5.3	5.9	15.3	9.4	9.1	9.3	7.6	7.1	7.5	7.5	4.4	4.9
Na_2O	1.0	0.4	2.9	4.6	4.0	0.3	3.0	0.5	0.9	0.9	1.1	1.1
K_2O	0.7	0.6	0.1	0.5	0.5	0.5	1.1	0.5	0.9	0.9	1.8	1.7
TOTAL	100.2	100.1	100.1	100.0	100.1	99.9	100.1	100.0	100.0	100.1	100.1	100.0
Mg/(Mg+ΣFe)	0.40	0.51	0.18	0.20	0.33	0.44	0.63	0.56	0.66	0.59	0.46	0.54

*Estimate, see Text.
†A = Andesite; B = Basalt.

30°, where the volcanoes lie about 90 to 150 km vertically above the seismic zone, amphibolite in the descending oceanic crust becomes unstable at depths of approximately 75 km, releasing H_2O that becomes available for melting. In the intervening regions with nearly flat dips, pressure–temperature conditions remain within the limits of amphibole stability, resulting in insufficient aH_2O to incur melting.

Acknowledgments

This research was supported through NSF grants EAR76-22330 and EAR73-00220-A02 to Boettcher.

Table 6b. Normative compositions (C.I.P.W.) of liquids in Table 6a

Norm	1	2	3	4	5	6	7	8	9	10	11	12	13	14	15	16	17	18	19	20	21	22	23	24
quartz	48.1	36.1	46.9	47.3	48.2	47.3	48.7	44.3	48.0	44.2	43.8	56.0	48.2	51.0	12.1	13.2	20.4	37.4	19.2	43.9	26.8	29.8	41.0	37.9
orthoclase	1.4	3.9	3.7	3.4	3.7	3.3	3.0	5.6	7.7	4.0	4.1	1.5	4.2	3.3	0.5	3.1	3.1	3.1	6.3	2.9	5.6	5.5	10.6	9.8
albite	5.7	6.8	12.7	6.7	5.8	5.9	5.0	5.9	5.8	9.2	8.3	1.9	8.6	3.6	24.3	39.0	33.4	2.7	25.1	4.6	7.4	7.6	9.5	9.7
anorthite	32.9	27.1	29.9	28.6	29.8	27.0	26.1	28.3	20.1	26.2	28.5	25.7	26.1	29.4	52.1	40.6	38.3	46.3	35.3	35.3	37.1	37.0	21.7	24.4
corundum	8.0	8.3	5.5	9.6	8.1	9.8	10.3	7.4	10.0	11.4	9.4	9.6	6.3	4.0	-	-	-	5.0	-	6.4	4.1	4.6	8.6	6.9
diopside	-	-	-	-	-	-	-	-	-	-	-	-	-	-	1.3	1.4	2.4	-	1.7	-	-	-	-	-
wo	-	-	-	-	-	-	-	-	-	-	-	-	-	-	(0.6)	(0.7)	(1.2)	-	(0.9)	-	-	-	-	-
en	-	-	-	-	-	-	-	-	-	-	-	-	-	-	(0.2)	(0.3)	(0.7)	-	(0.7)	-	-	-	-	-
fs	-	-	-	-	-	-	-	-	-	-	-	-	-	-	(0.5)	(0.4)	(0.5)	-	(0.1)	-	-	-	-	-
hypersthene	2.3	14.4	0.6	3.2	3.3	5.2	5.4	5.6	5.1	3.3	4.3	3.4	4.1	5.9	-	-	-	2.3	8.8	4.4	13.8	9.9	4.1	7.0
en	(1.2)	(11.5)	(-)	(2.3)	(2.2)	(4.0)	(4.3)	(4.2)	(4.3)	(2.3)	(3.5)	(2.4)	(2.6)	(4.4)	-	-	-	(2.3)	(7.6)	(3.9)	(12.5)	(8.9)	(3.9)	(6.0)
fs	(1.1)	(2.9)	(0.6)	(0.9)	(1.1)	(1.2)	(1.1)	(1.4)	(0.8)	(1.0)	(0.8)	(1.0)	(1.5)	(1.5)	-	-	-	(0.0)	(1.2)	(0.5)	(1.3)	(1.0)	(0.2)	(1.0)
wollastonite	-	-	-	-	-	-	-	-	-	-	-	-	-	-	9.3	1.9	1.6	-	-	-	-	-	-	-
magnetite	1.2	2.9	0.6	1.0	1.1	1.3	1.3	2.1	1.9	1.2	1.1	1.4	1.8	2.1	0.5	0.6	0.6	1.4	2.4	1.5	3.0	3.0	2.2	2.5
ilmenite	0.5	0.7	0.1	0.2	0.1	0.1	0.2	0.8	1.3	0.5	0.4	0.6	0.7	0.7	-	0.2	0.2	1.6	1.3	1.1	2.3	2.6	2.3	1.8

References

Allen, J. C., A. L. Boettcher and G. Marland (1975) Amphiboles in andesite and basalt: I. Stability as a function of P-T-f_{O_2}. *Am. Mineral.*, *60*, 1069–1085.

Anderson, A. T. (1974) Before-eruption H_2O content of some high-alumina magmas. *Bull. Volcanol.*, *37*, 530–552.

Apted, M. J., A. L. Boettcher and B. O. Mysen (1977) *In situ* measurements of the distribution of Ce, Sm, and Tm between garnet/melt and amphibole/melt, utilizing beta isotopes (abstr.). In papers presented to the *International Conference on Experimental Trace Element Geochemistry*, 1.

Barazangi, M. and B. L. Isacks (1976) Spatial distribution of earthquakes and subduction of the Nazca Plate beneath South America. *Geology*, *4*, 686–692.

Bence, A. E. and A. L. Albee (1968) Empirical correction factors for the electron-microanalysis of silicates and oxides. *J. Geol.*, *76*, 382–403.

Boettcher, A. L. (1973) Volcanism and orogenic belts—the origin of andesites. *Tectonophysics*, *17*, 223–240.

——— (1977) The role of amphiboles and water in circum-Pacific volcanism. In M. H. Manghnani and S. Akimoto, Eds., *High-Pressure Research, Applications in Geophysics*, p. 107–125. Academic Press, London.

———, B. O. Mysen and J. C. Allen (1973) Techniques for the control of water fugacity and oxygen fugacity for experimentation in solid-media high-pressure apparatus. *J. Geophys. Res.*, *78*, 5898–5902.

Bowen, N. L. (1928) *The Evolution of the Igneous Rocks.* Princeton University Press, Princeton.

Cawthorn, R. G. and M. J. O'Hara (1976) Amphibole fractionation in calc-alkaline magma genesis. *Am. J. Sci.*, *276*, 309–329.

Frey, F. A., W. B. Bryan and G. Thompson (1974) Atlantic Ocean floor: geochemistry of basalts from legs 2 and 3 of the Deep Sea Drilling Project. *J. Geophys. Res.*, *79*, 5507–5527.

Hart, S. R. (1969) K, Rb, Cs contents and K/Rb, K/Cs ratios of fresh and altered submarine basalts. *Earth Planet. Sci. Lett.*, *6*, 295–303.

Helz, R. T. (1976) Phase relations of basalts in their melting ranges at P_{H_2O} = 5 kb. Part II. Melt compositions. *J. Petrol.*, *17*, 139–193.

Hill, R. E. T. and A. L. Boettcher (1970) Water in the Earth's mantle: Melting curves of basalt-water and basalt-water-carbon dioxide. *Science*, *167*, 980–982.

Leake, B. E. (1968) A catalog of analyzed calciferous and subcalciferous amphiboles together with their nomenclature and associated minerals. *Geol. Soc. Am. Spec. Pap. 68.*

Lopez-Escobar, L., F. A. Frey and M. Vergara (1976) Andesites from central-south Chile: Trace element abundances and petrogenesis. In O. G. Ferran, Ed., *Proceedings of the Symposium on Andean and Antarctic Volcanology Problems*, p. 725–761. Giannini and Figli, Naples, Italy.

Mysen, B. O. and A. L. Boettcher (1975) Melting of a hydrous mantle: II. Geochemistry of crystals and liquids formed by anatexis of mantle peridotite at high pressures and high temperatures as a function of controlled activities of water, hydrogen, and carbon dioxide. *J. Petrol.*, *16*, 549–593.

Ringwood, A. E. (1974) The petrological evolution of island arc systems. *J. Geol. Soc. Lond.*, *130*, 183–204.

Stern, C. R. and P. J. Wyllie (1975) Effect of iron absorption by noble-metal capsules on phase boundaries in rock-melting experiments at 30 kilobars. *Am. Mineral.*, *60*, 681–689.

Thorpe, R. S., P. J. Potts and P. W. Francis (1976) Rare earth data and petrogenesis of andesite from the north Chilean Andes. *Contrib. Mineral. Petrol.*, *54*, 65–78.

Manuscript received, November 1, 1977; accepted for publication, June 1, 1978.

The following material did not appear in the original publication.

Table . Experimental Results

$X^V_{H_2O}$	Pres Kbars	Temp ^0C	Run Number†	Duration hours	Phase Assemblage*
			Andesite		
0.25	10	800	A 499	22.3	Pl,Opx,Cpx,Op
0.25	10	820	A 501	22.8	Pl,Opx,Cpx,Op
0.25	10	860	A 503	22.0	Pl,Opx,Cpx,Op,(QM)
0.25	10	900	A 505	21.5	Pl,Opx,Cpx,Op,QM
0.25	10	920	A 508	21.8	L,Pl,Opx,Cpx,Op
0.25	10	940	A 507	22.2	L,Pl,Opx,Cpx,Op
0.25	10	1080	A 502	5.5	L,Pl,Op,(Cpx),(Opx)
0.25	10	1100	A 498	5.3	L,Pl,Op,(Cpx),?Opx
0.25	10	1120	A 500	5.8	L,Op
0.25	13	820	A 420	23.0	Pl,Opx,Cpx,Op
0.25	13	860	A 509	4.0	Pl,Opx,Cpx,Op
0.25	13	860	A 504	22.0	Pl,Opx,Cpx,Op
0.25	13	880	A 510	4.0	Pl,Opx,Cpx,Op
0.25	13	880	A 506	21.7	Pl,Opx,Cpx,Op
0.25	13	900	A 381	3.0	L,Pl,Opx,Cpx,Op
0.25	13	900	A 524	23.5	L,Pl,Opx,Cpx,Op
0.25	13	940	A 376	3.3	L,Pl,Opx,Cpx,Op
0.25	13	980	A 364	3.0	L,Pl,Opx,Cpx,Op
0.25	13	1020	A 386	3.3	L,Pl,Opx,Cpx,Op
0.25	13	1060	A 389	3.0	L,Pl,Opx,Cpx,Op
0.25	13	1100	A 393	3.0	L,Cpx,Op
0.25	13	1120	A 421	3.0	L,Op
0.50	10	940	A 391	3.2	L,Am,Pl,Opx,Cpx,Op
0.50	10	960	A 399	3.3	L,Am,Pl,Opx,Cpx,Op
0.50	10	980	A 405	3.5	L,Pl,Opx,Cpx,Op
0.50	10	1000	A 491	4.5	L,Pl,Cpx,Op,(QM)
0.50	10	1020	A 380	3.3	L,Pl,Op,QM
0.50	10	1040	A 377	3.4	L,Op,QM
0.50	13	920	A 365	3.0	L,Am,Pl,Opx,Cpx,Op
0.50	13	940	A 366	3.1	L,Am,Pl,Opx,Cpx,Op
0.50	13	960	A 281	3.0	L,Pl,Opx,Cpx,Op
0.50	13	980	A 357	3.0	L,Pl,Opx,Cpx,Op
0.50	13	1000	A 372	3.0	L,Pl,Cpx,Op,QM
0.50	13	1020	A 353	3.0	L,Pl,Cpx,Op
0.50	13	1040	A 349	3.0	L
0.50	16	920	A 388	3.0	L,Am,Opx,Cpx,Op
0.75	10	900	A 390	3.3	L,Am,Pl,Opx,Op,QM
0.75	10	920	A 490	4.5	L,Am,Pl,Opx,Op,QM
0.75	10	940	A 492	3.8	L,Am,Opx,Op,QM
0.75	10	960	A 383	3.5	L,Am,Opx,Op,QM
0.75	10	980	A 379	3.0	L,Op,QM
0.75	13	900	A 489	3.5	L,Am,Opx,Op,QM
0.75	13	920	A 398	3.2	L,Am,Opx,Op
0.75	13	940	A 386	3.3	L,Am,Opx,Op,QM

0.75	13	940	A 486	22.5	L,Am,Opx,Op,QM
0.75	13	960	A 370	3.0	L,Am,Opx,Op,QM
0.75	13	980	A 375	3.0	L,Op,QM
0.75	14	920	A 493	6.3	L,Am,Opx,Op,QM
0.75	15	920	A 494	5.5	L,Am,Opx,Op,(Cpx),QM
0.75	16	940	A 460	23.5	L,Am,Cpx,Opx,Op,(QM)
0.75	16	980	A 456	2.5	L,Op,QM
0.75	17	960	A 495	1.5	L,Am,Cpx,Opx,Op,QM
0.75	18	940	A 458	24.0	L,Am,Cpx,Op,(Opx),QM
0.75	19	940	A 487	3.2	L,Am,Cpx,Op,Opx,QM
0.75	20	940	A 459	24.3	L,Am,Cpx,Op,(Opx),QM
0.75	21	940	A 457	22.0	L,Ga,Cpx,Op,(Opx),QM
0.75	22	940	A 455	22.5	L,Ga,Cpx,Op,QM
1.0	10	940	A 227	3.0	L,Am,Op,QM
1.0	10	960	A 222	3.0	L,Op,QM
1.0	13	880	A 72	5.2	L,Am,Pl,Op
1.0	13	920	A 68	3.2	L,Am,Op
1.0	13	940	A 70	4.0	L,Am,Op,QM
1.0	13	960	A 223	4.3	L,Op,QM
1.0	16	960	A 452	24.2	L,Op,QM
1.0	17	920	A 519	3.0	L,Am,Op,QM
1.0	18	920	A 522	3.0	L,Am,Op,QM
1.0	19	920	A 448	22.0	L,Am,Op,(Cpx)
1.0	20	920	A 453	23.3	L,Am,Cpx,Op,QM
1.0	21	920	A 454	23.5	L,Am,Cpx,Op,QM
1.0	22	920	A 450	23.5	L,Ga,Cpx,Op,QM

** Reversals

0.50	13	1000	A 531R	4.5	(see run #372)
	13	925		5.5	L,Am,Pl,Cpx,Opx,Op
0.75	13	980	A 532R	3.3	(see run #375)
	13	945		3.0	L,Am,Opx,Op
0.75	21.5	940	A 533R	21.8	(see run #457)
	19.5	940		22.0	L,Cpx,Op,Am,Ga,Opx
1.0	13	960	A 534R	2.1	(see run #223)
	13	925		4.0	L,Am,Op,QM
1.0	22.5	920	A 535R	23.0	(see run #450)
	20.5	920		23.8	L,Am,Ga,Cpx,Op,QM
0.25	13	1125	A 590R	3.1	(see run #421)
	13	1095		4.2	L,Cpx,Op,(Pl)
0.50	13	1045	A 589R	3.3	(see run #349)
	13	1015		4.0	L,Cpx,Op,Pl

Basalt

0.25	10	1020	B 465	23.0	L,Am,Cpx,Pl,Op,(Opx),(QM)
0.25	10	1040	B 473	22.5	L,Am,Cpx,Op,(QM)
0.25	10	1060	B 475	22.5	L,Cpx,Op,(QM)
0.25	10	1180	B 488	6.0	L,Cpx,Op,QCpx
0.25	10	1200	B 484	7.0	L,Op,QCpx
0.25	10	1220	B 483	6.0	L,Op,QCpx
0.25	13	960	B 444	22.7	L,Am,Cpx,Pl,Op,(Opx),(QM)
0.25	13	1000	B 439	3.0	L,Am,Cpx,Pl,Op,(Ol),(Opx),(QM)

0.25	13	1000	B 445	22.1	L,Am,Cpx,Pl,Op,(Ol),(Opx),(QM)
0.25	13	1020	B 477	22.5	L,Am,Cpx,Pl,Op,(Ol),(Opx),(QM)
0.25	13	1040	B 447	23.7	L,Am,Cpx,Op,(Ol),(QM)
0.25	13	1060	B 471	22.5	L,Cpx,Op,(QM)
0.25	13	1060	B 485	3.6	L,Cpx,Op,(QM)
0.25	13	1080	B 464	22.5	L,Cpx,Op,(QM)
0.25	13	1120	B 474	22.5	L,Cpx,Op,(QM)
0.25	13	1160	B 476	22.5	L,Cpx,Op,(QM)
0.25	13	1200	B 478	9.3	L,Cpx,Op,(QM)
0.25	13	1220	B 481	7.0	L,Op,QCpx
0.25	13	1240	B 479	11.0	L,Op,QCpx
0.25	15	1000	B 553	5.5	L,Cpx,Am,Pl,Op
0.25	15	1020	B 554	5.5	L,Cpx,Am,Pl,Op
0.25	15	1040	B 555	4.0	L,Cpx,Am,Pl,Op
0.25	15	1060	B 556	5.0	L,Cpx,Op,(Ol),(Pl)
0.25	16	1020	B 551	5.5	L,Cpx,Ga,Op
0.25	16	1040	B 548	5.5	L,Cpx,Ga,Op
0.25	16	1060	B 541	5.3	L,Cpx,Op
0.25	16	1200	B 544	4.0	L,Cpx,Op,QCpx
0.25	16	1220	B 547	4.3	L,Op,QCpx
0.25	16	1240	B 545	4.3	L,Op,QCpx
0.25	17	1020	B 546	25.5	L,Cpx,Ga,Op
0.25	18	1020	B 543	22.5	L,Cpx,Ga,Op
0.25	19	1020	B 550	22.5	L,Cpx,Ga,Op
0.50	10	1000	B 387	3.1	L,Am,Cpx,Op
0.50	10	1020	B 392	3.0	L,Am,Cpx,Op,QM
0.50	10	1040	B 382	3.0	L,Cpx,Op,QM
0.50	10	1120	B 402	3.3	L,Cpx,Op
0.50	10	1140	B 404	3.5	L,Cpx,Op
0.50	10	1160	B 410	3.3	L,Op,QCpx,QM
0.50	13	1000	B 360	3.0	L,Am,Cpx,Op,QM
0.50	13	1040	B 361	3.0	L,Am,Cpx,Op,(Ol),QM
0.50	13	1060	B 369	3.0	L,Cpx,Op,QM,QAm
0.50	13	1100	B 371	3.0	L,Cpx,Op,QM,QAm
0.50	13	1120	B 378	3.0	L,Cpx,Op,QM
0.50	13	1140	B 374	3.1	L,Op,QCpx
0.50	16	1020	B 433	22.5	L,Am,Cpx,Op,QM
0.50	16	1040	B 440	3.0	L,Cpx,Op,QM
0.50	16	1060	B 428	3.0	L,Cpx,Op,QM
0.50	16	1100	B 441	3.0	L,Cpx,Op,QM
0.50	16	1120	B 431	3.0	L,Op,QCpx,QM
0.50	17	1020	B 422	22.0	L,Cpx,Am,Ga,Op,QM
0.50	18	1020	B 432	22.0	L,Cpx,Ga,Op,QM
0.50	19	1020	B 414	22.0	L,Cpx,Ga,Op,QM
0.50	21	1020	B 409	22.7	L,Cpx,Ga,Op,QM
0.75	10	980	B 437	3.0	L,Am,Cpx,Op,QM
0.75	10	1000	B 435	3.0	L,Cpx,Op,QM
0.75	10	1060	B 438	3.0	L,Cpx,Op,QM
0.75	10	1080	B 436	3.2	L,Op,QCpx,QAm,QM
0.75	10	1100	B 434	3.0	L,Op,QCpx,QAm,QM
0.75	13	980	B 415	3.4	L,Am,Cpx,Pl,Op,QM
0.75	13	1000	B 418	3.3	L,Am,Cpx,Op,QM
0.75	13	1020	B 413	3.1	L,Cpx,Op,QM,QCpx

0.75	13	1060	B 411	4.0	L,Cpx,Op,QM,QCpx,QAm
0.75	13	1080	B 427	3.7	L,Cpx,Op,QM,QCpx,QAm
0.75	13	1100	B 426	3.0	L,Op,QM,QCpx,QAm
0.75	18	980	B 513	23.0	L,Am,Cpx,Op
0.75	18	1000	B 514	5.8	L,Am,Cpx,Op
0.75	18	1020	B 517	3.2	L,Cpx,Op,(QM)
0.75	19	980	B 511	24.3	L,Am,Cpx,Ga,Op
0.75	20	980	B 512	22.3	L,Cpx,Ga,Op
1.0	10	980	B 248	3.2	L,Cpx,Am,Op,QM
1.0	10	1000	B 272	3.3	L,Cpx,Op,QM
1.0	10	1060	B 515	3.0	L,Cpx,Op,QM
1.0	10	1080	B 525	1.2	L,Op,QM
1.0	10	1100	B 516	3.3	L,Op,QM
1.0	13	950	B 394	4.0	L,Cpx,Am,Op,QM
1.0	13	980	B 77	4.5	L,Cpx,Am,Op
1.0	13	1000	B 73	4.9	L,Cpx,Op
1.0	13	1020	B 69	4.8	L,Cpx,Op
1.0	13	1040	B 61	5.0	L,Cpx,Op,QM
1.0	13	1060	B 82	4.5	L,Cpx,Op,QM,QAm
1.0	13	1080	B 80	4.5	L,Op,QM,QCpx,QAm
1.0	17	1000	B 462	11.3	L,Cpx,Op,QM
1.0	19	940	B 451	22.5	L,Am,Cpx,Op,QM
1.0	20	940	B 461	22.0	L,Am,Cpx,Op,QM
1.0	21	940	B 449	22.5	L,Cpx,Ga,Op,QM

** Reversals

0.25	13	1120	B 526R	3.8	(see run #474)
	13	1025		17.8	L,Cpx,Am,Op
0.25	19.5	1020	B 557R	23.0	(see run #550)
	14.5	1020		23.3	L,Cpx,Op,Ga,Am
0.50	15	1130	B 442R	3.3	(see run #431)
	15	1020		19.3	L,Cpx,Am,Op,QM
0.50	18.5	1015	B 443R	22.5	(see run #432)
	15.5	1015		23.8	L,Cpx,Am,Op,QM
0.75	13	1100	B 537R	2.3	(see run #426)
	13	985		3.0	L,Cpx,Am,Op
0.75	20.5	980	B 538R	23.1	(see run #512)
	17.5	980		23.3	L,Cpx,Am,Ga,Op,QM
1.0	13	1070	B 530R	2.3	(see run #82)
	13	960		3.7	L,Cpx,Am,Op,QM
1.0	21.5	940	B 539R	23.3	(see run #449)
	19.5	940		23.8	L,Cpx,Am,Op,QM

0.25	13	1225	B 587R	4.5	(see run #481)
	13	1195		3.5	L,Cpx,Op,QM
0.25	16	1225	B 585R	4.0	(see run #547)
	16	1195		4.0	L,Cpx,Op,QM
0.50	13	1145	B 583R	3.8	(see run #374)
	13	1115		3.4	L,Cpx,Op,QM
0.50	16	1125	B 584R	4.6	(see run #431)
	16	1095		3.5	L,Cpx,Op,QM
0.75	10	1085	B 582R	5.0	(see run #436)
	10	1055		3.5	L,Cpx,Op,QM
0.75	13	1105	B 581R	3.0	(see run #426)
	13	1075		3.4	L,Cpx,Op,QM
1.0	10	1085	B 588R	3.2	(see run #525)
	10	1055		3.3	L,Cpx,Op,QM
1.0	13	1085	B 586R	4.0	(see run #80)
	13	1055		3.5	L,Cpx,Op,QM

Abbreviations: *Am = amphibole; Cpx = clinopyroxene; Ga = garnet; L = glass interpreted to be quenched liquid; M = micaceous mineral; Ol = olivine; Op = opaque mineral; Opx = orthopyroxene; Pl = plagioclase; q = interpreted to have crystallized during the quench; ? = questionable; ( ) = trace amount*

* *All assemblages include vapor*

† *Run numbers preceded by A employed andesite as a starting material; those preceded by B used basalt.*

** *See text for description of reversal procedure*

End of supplemental material.